The Effect of Annealing Temperature of ZnO Compact Layer and TiO_2 Mesoporous on Photo-Supercapacitor Performance

IOP Conf. Series: Materials Science and Engineering **515** (2019) 012006 doi:10.1088/1757-899X/515/1/012006

The Effect of Annealing Temperature of ZnO Compact Layer and TiO_2 Mesoporous on Photo-Supercapacitor Performance

Thathit Suprayogi[1], Moh. Zahir Masrul[1], Markus Diantoro[1,2,*], Ahmad Taufiq[1,2], Abdulloh Fuad[1,2], Arif Hidayat[1,2]

[1] Department of Physics, Faculty of Mathematics and Natural Sciences, Universitas Negeri Malang, Jl. Semarang 5 Malang 65145, Indonesia
[2] Center of Advanced Material for Renewable Energy (CAMRY), Universitas Negeri Malang, Jl. Semarang 5, Malang 65145, Indonesia

*Corresponding author's email: markus.diantoro.fmipa@um.ac.id

Abstract. Photo-supercapacitor is a combination of solar cells and supercapacitor which intensively being developed. Photo-supercapacitor performance is influenced by the efficiency of solar cells and storing and releasing capacity of supercapacitors. Any types of either solar section or supercapacitor sections could be used. In the DSSC solar cell, one of the influential variables is the performance of the photoanode. The photoanode with semiconducting metal oxides play a role in charges mobility and light absorption process, which are influenced by crystal morphology and structures. The common metal oxides used are ZnO and TiO_2 which show high electron mobility, wide band gap, and good optical properties. This work is designed to investigate the effect of annealing temperature of the composite layer of ZnO and mesoporous TiO_2 on structure, morphology, optical absorption, and photo-supercapacitor performance. The ZnO compact layer was deposited onto the FTO substrate by a spin coating method with various annealing temperature. The mesoporous TiO_2 layer was deposited on top of the ZnO compact layer by means of screen printing method. The construction of photo-supercapacitor model comprises DSSC and $BaTiO_3$-PVDF symmetric supercapacitor which integrated by using aluminum substrate. Characterization was done using XRD, SEM, UV-Vis, and I-V solar simulators for the performance of photo-supercapacitor.

Keywords: Photo-supercapacitor, annealing temperature, ZnO compact layer, mesoporous TiO_2.

1. Introduction

Generation and storage electrical energy device such as photo-supercapacitor have been the subject of many research interest in recent years [1–4]. Photo-supercapacitor is interesting to be developed because of it's perform the combination of solar cell and supercapacitor simultaneously, so other conventional devices and size can be reduced [2–6]. One of the photo-supercapacitor is a combination of dye-sensitized solar cell (DSSC) and supercapacitor based on electric double layer capacitors (EDLC) [1,4,6–10]. The combination of those two devices may affect not only of each section but also the interconnection between them.

Several sections which influenced the DSSC efficiency are metal oxide at photoanode, photosensitizer (dye), electrolyte, and counter electrodes [11–14]. The photoanode electrode with metal

oxide effect on collecting and transferring electrons from the dye to transparent conductive oxide (TCO). There are many studies have been conducted to optimize metal oxide materials with various n-type semiconductors such as TiO_2, ZnO, and SnO_2 [12,15–19]. TiO_2 is the main candidate for DSSC photoanode because of its wide band gap, thermal stability, non-toxic, and stable under sunlight [12,20,21]. In addition, TiO_2 in nanometer size and porous morphology not only good for dye absorption but also has electron interfacial recombination faster than other metal oxides [22–24]. However, TiO_2 shows quite low electron mobility, which has an impact on conversion efficiency [25]. One way to increase electron mobility in TiO_2 needs to be modified its morphology or composites with other metal oxides.

The morphological structure of mesopore TiO_2 apply as photoanodes DSSC can improve conversion efficiency, but the interface between mesopore TiO_2 with TCO such as indium tin oxide (ITO) or fluorine tin oxide (FTO) is low [26,27]. It is necessary to modify the photoanode structure by introducing a compact layer such as ZnO between mesopore TiO_2 and TCO. In addition, ZnO can increase electron mobility in DSSC photoanodes because ZnO has high electron mobility (115-155 $cm^2V^{-1}s^{-1}$) [28]. Many works have been performed in combining TiO_2 with ZnO with core-shell structure [29], composite TiO_2 nanoparticles with ZnO nanorod [18], ZnO nanowire / TiO_2 core-shell nanosheet [30], compact layers TiO_2 [31], and ZnO nanoflower composites with TiO_2 nanorod [28]. Those efforts aimed to enhance the DSSC efficiency.

The efficiency energy conversion is expected to increase by combining TiO_2 mesopore with compact layer ZnO at DSSC's photoanode. In the long run, it affects the performance of photo-supercapacitor. One type of EDLC supercapacitor by using $BaTiO_3$ is exciting to be studied. $BaTiO_3$ is a ferroelectric ceramic which exhibits an excellent of pyro, piezo, and capacitance properties [32,33]. However, since ceramic is a brittle and rigid material which need to be combined with polymers such as polyvinylidene fluoride (PVDF) which has a flexible, easily composited, and has good capacitance [32]. One type of photo-supercapacitor with the best design is three photo-supercapacitor electrodes exhibit maximum voltage, high power, and energy density, have high efficiency, fast charge and discharge, and durable [1,4,7,34]. The interface between mesoporous TiO_2 with TCO and electron mobility in DSSC photoanodes for mesopore TiO_2 is too low to be implemented. We report three gates photo-supercapacitor performance by implementing a compact layer ZnO with mesoporous TiO_2 and ZnO rods combined with symmetric supercapacitor PVDF-$BaTiO_3$.

2. Methods

An FTO-glass substrate was firstly cleaned following a standard protocol. Compact layer ZnO was deposited on FTO-glass substrate using a spin coating method. ZnO solution was prepared using Zinc acetate dehydrate ($Zn(CH_3COO)_2.2H_2O$) Sigma-Aldrich 99% in ethanol and added 0.5 mL Monoethanolamine (MEA) Sigma-Aldrich 99% as a stabilizer. Mesoporous TiO_2 was layered on compact layer ZnO by screen printing method. Mesoporous TiO_2 paste was prepared by TiO_2 (P25) Sigma-Aldrich 99%, Sodium dodecyl sulfate (SDS), Polyethylene glycol 6000 (PEG) in distilled water. The ZnO solution was deposited on the mesoporous TiO_2 layer by a spin coating method. FTO/ZnO/ TiO_2 -ZnO was dried at 100 °C followed by annealed for a various temperature of 300, 350, and 400 °C for 2 hours. Photoanode electrode FTO/ZnO/ TiO_2 -ZnO with the codes for each annealing temperature were ZnTi 300, ZnTi 350, and ZnTi 400 respectively. The counter electrode was prepared by carbon tape at aluminum foil substrate, then heated at 250 °C for 30 min.

Supercapacitor was designed by symmetry PVDF-BaTiO3 on aluminum foil substrate with hydrogel electrolyte and Polytetrafluoroethylene (PTFE) as a separator. A PVDF-$BaTiO_3$ paste was deposited on an aluminum substrate by slip casting. Hydrogel electrolyte was prepared by polyvinyl alcohol (PVA), potassium hydroxide (KOH), and potassium iodide (KI) in distilled water. Photo-supercapacitor was designed by modifying the design as described by Lau et al. [1] is represented by Figure 1. DSSC was constructed by sandwiching photoanode and counter electrode with quercetin and beta-carotene dye and I^-/I^{3-} electrolyte. DSSC was combined with symmetric supercapacitor become photo-supercapacitor.

The structure and morphology of the nanostructured photoanodes were characterized by the use of a scanning electron microscopy (SEM Merk FEI, Type: Inspect-S50). The X-ray diffraction (XRD) pattern was recorded using an XRD E'Xpert Pro PANalytical with Cu-kα (λ= 1.54060 Å, 35 mA, dan 40 kV) at 2θ in the range of 10-80°. Optical properties of the photoanode film were scanned at a wavelength of 200-800 nm with UV-Vis UV1700. Photovoltaic and photo-charging were measured for current vs. time (I-t) and voltage vs. time (V-t) by Keithley 6515B Electrometer under 20 mW/cm2 illumination.

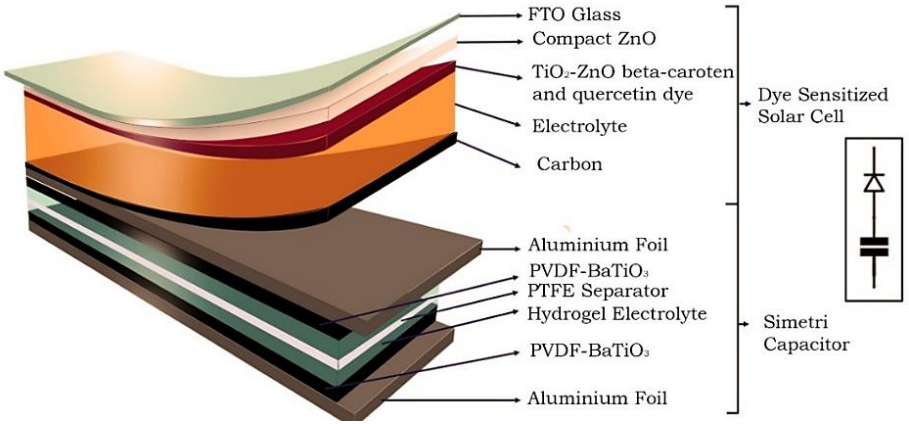

Figure 1. Schematic of photo-supercapacitor device modified from ref. [1].

3. Results and Discussion

XRD pattern of the photoanode electrode with various annealing temperature shows in Figure 2. All the Bragg peaks in the XRD pattern can be indexed well to the anatase TiO_2phase COD 2310710 [35], ZnO phase COD 9004178 [36], and FTO JCPDS card no. 01-0625 [37]. Anatase TiO2 has a tetragonal crystal system with $I4_1$/amd space group and ZnO crystallized under $P6_3$mc space group. The variation in the annealing temperature does not look significant for the ZnO phase due to compact layer ZnO at the bottom layer [37,38].

Rietveld refinement was calculated for the composite of ZnO and TiO_2 (later indicated as ZnTi) 400 XRD pattern using GSAS software shows in Figure 3. It is shown that TiO_2 lattice parameters fall to $a = b = 3.750$ Å and $c = 9.5053$ Å. The obtained lattice parameters of ZnO phase is $a = b = 3.2494$ Å dan $c = 5.2038$ Å. Reliability Rietveld refinement between calculation and experiment data ZnTi 400 are $Rp = 0.1999$, $Rwp = 0.3005$, dan $\chi^2 = 1.413$. Figure 3 (b) and (c) shows a crystal structure of TiO_2 and ZnO respectively using VESTA software.

XRD pattern of supercapacitor electrode with PVDF-$BaTiO_3$ is shown in Figure 4. All the diffraction peak in the XRD pattern is appropriate with PVDF phase CSD LILXIN05, $BaTiO_3$ phase COD 4124842, and Aluminum foil. $BaTiO_3$ phase fit to cubic crystal structure with Pm-3m space group and PVDF phase has orthorhombic crystal system with Cm2m space group. Rietveld refinement of XRD pattern has been done using GSAS software. Kisi parameter of $BaTiO_3$ phase is $a = b = c = 4.025419$ Å and PVDF phase are $a = 8.5822$, $b = 4.9102$, $c = 2.559$ Å. Good reliability Rietveld refinement are $Rp = 0.2741$, $Rwp = 0.1906$, dan $\chi^2 = 1.483$. Crystal structure of $BaTiO_3$ and PVDF shows in Figure 4 (b) and (c) respectively. Equation 1 represents the Scherrer formula used to calculate the crystal size of $BaTiO_3$ is 41.3 nm.

$$d = \frac{k\lambda}{\beta \cos\theta} \tag{1}$$

where d is crystal size, k is shape factor, λ is wavelength Cu-kα, β is full width at half maximum (FWHM), and θ is the Bragg position.

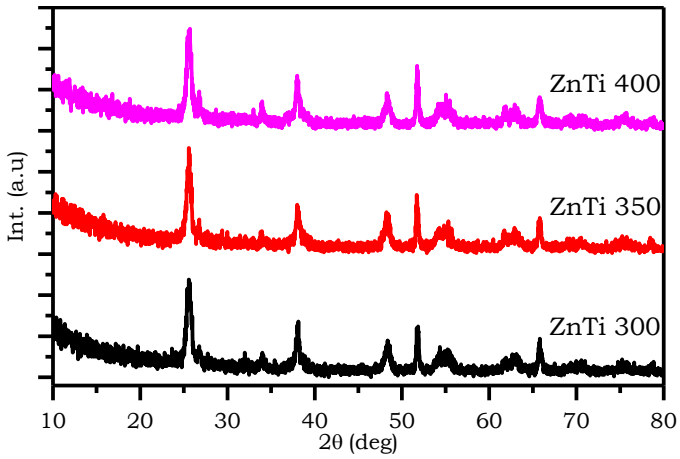

Figure 2. XRD pattern of photoanode electrode with various annealing temperature

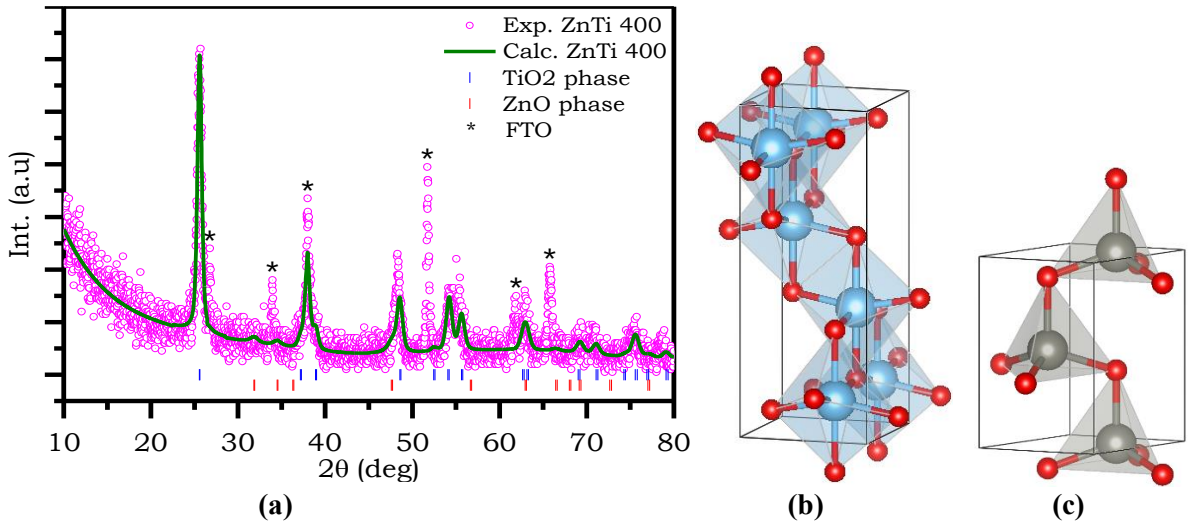

Figure 3. Rietveld refinement of ZnTi 400 using GSAS (a), crystal structure of TiO_2 (b) and ZnO (c)

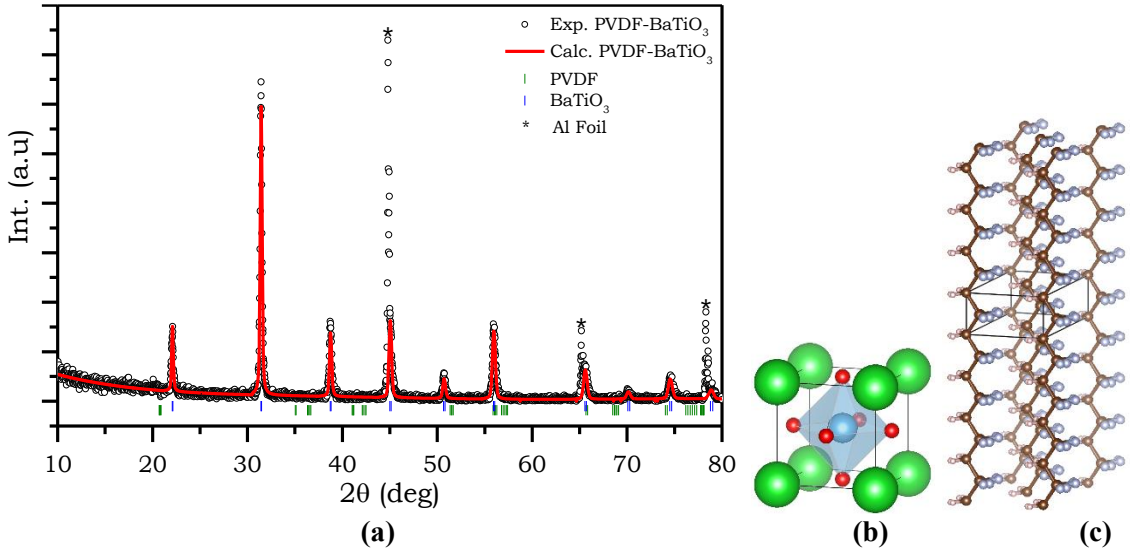

Figure 4. XRD pattern with Rietveld refinement using GSAS of PVDF-$BaTiO_3$ (a), crystal structure of $BaTiO_3$ (b), and PVDF (c)

Figure 5 shows the top-view SEM of the photoanode electrode at the various annealing temperature. The morphology of TiO_2 is mesoporous and ZnO growth to nanorods. The annealing temperature is linearity influencing crystal growth of ZnO nanorods diameter is shown in insert picture Figure 5. Crystal growth of ZnO at compact layer increase interfacing between mesoporous TiO_2 and FTO substrate to provide electron mobility increase [31,39,40].

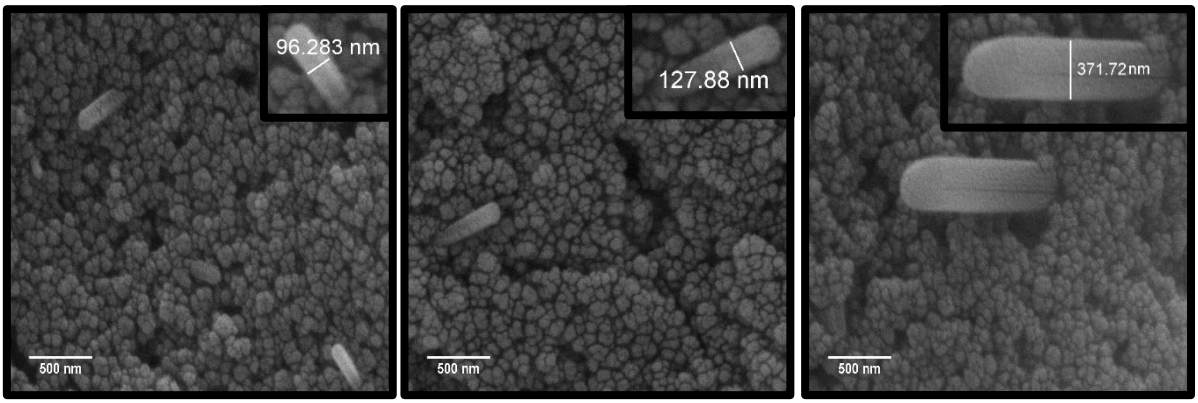

(a) **(b)** **(c)**

Figure 5. SEM image of photoanode electrode with various annealing temperature 300 (a), 350 (b), and 400 °C (c)

Figure 6 (a) shows SEM image top-view of supercapacitor electrode (PVDF-$BaTiO_3$) on aluminum foil substrate. PVDF-$BaTiO_3$ has a uniform particle size. The porosity analysis has been done using previous work [41] by approximation area under the curve that density porosity is 0.70. The porous morphological of supercapacitor electrode can increase the capacitance of the supercapacitor [42].

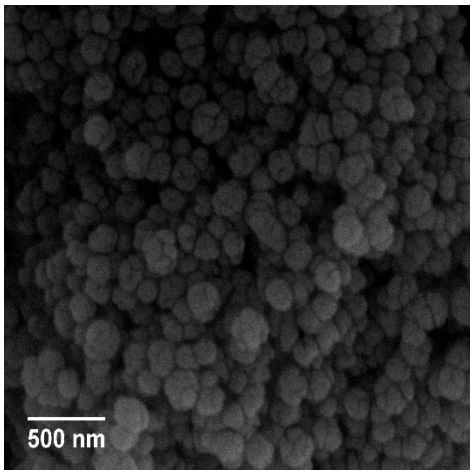

Figure 6. SEM image of PVDF-$BaTiO_3$

The optical properties of the photoanode electrode with various layer and the annealing temperature were characterized using UV-Vis at a wavelength between 200-800 nm shows in Figure 7a and Figure 8a respectively. The absorbance at semiconductor material is related to the energy used by an electron to excite from valence band to conduction band [43]. The direct transition of the electron is expressed by Equation 2 [11].

$$(\alpha h\upsilon) = A(h\upsilon - Eg)^{1/2} \tag{2}$$

where α, $h\upsilon$, Eg, and A are absorbance coefficient, photon energy, band gap, and constant respectively. Tauc plot method was used to analyze band gap by intercept at x-axis from graph $h\upsilon$ vs. $(\alpha h\upsilon)^2$ [44].

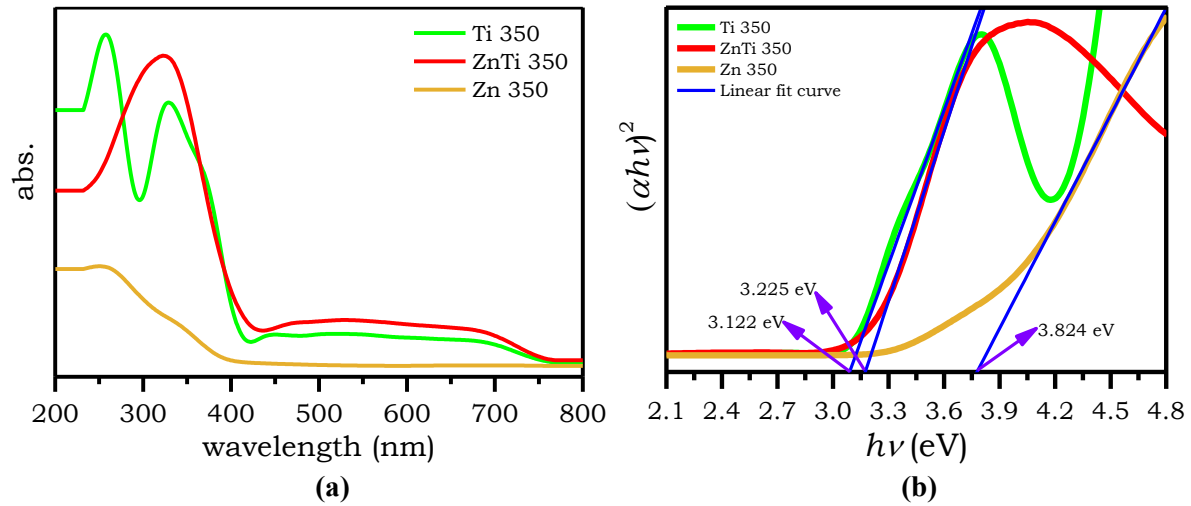

Figure 7. Absorbance spectra of TiO_2 without compact layer ZnO (Ti 350), Compact layer ZnO (Zn 350), and TiO_2-ZnO with compact layer ZnO (ZnTi 350) on FTO substrate (a), and Tauc plot (b)

Figure 7a represents spectral absorbance of a various layer that indicates decreasing absorbance coefficient at wavelength 400-800 nm. This phenomenon indicates that photon energy was used by the electron to excite from valence band to conduction band. The magnitude energy corresponding to the band gap of each semiconductor. The compact layer ZnO has *Eg* = 3.824 eV eV [45] and TiO_2 layer without compact layer ZnO has *Eg* = 3.122 eV [46,47]. TiO_2-ZnO layer with compact layer ZnO has Eg = 3.225 eV.

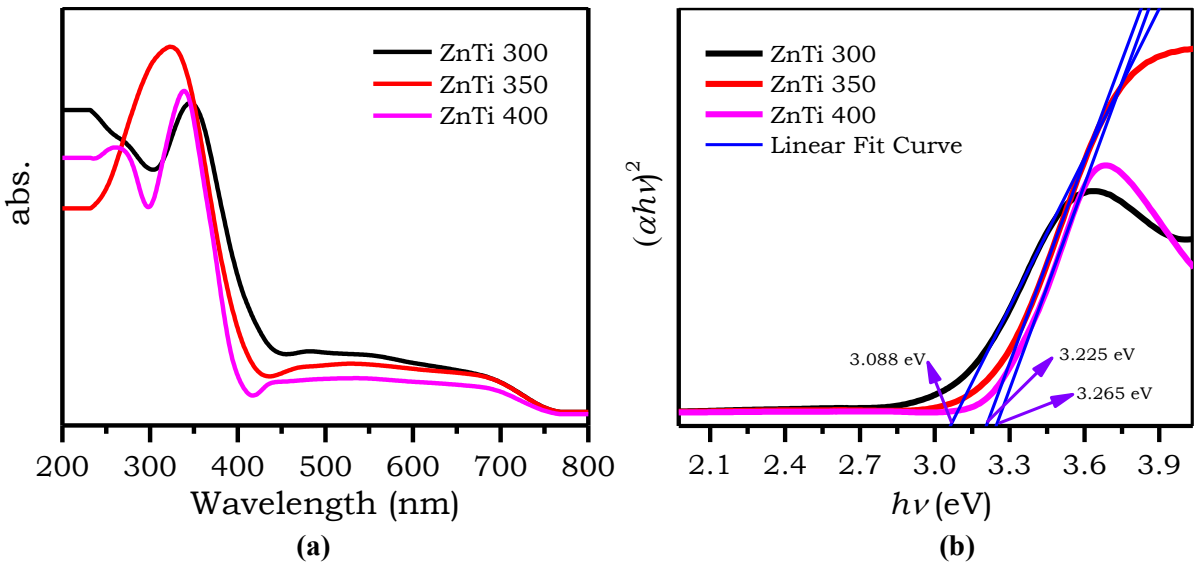

Figure 8. Absorbance spectra of photoanode electrode (ZnTi) with various annealing temperature (a) and Tauc plot for band gap calculation (b)

Figure 8a shows the absorbance spectral photoanode electrode of ZnTi with various annealing temperature. There is a shift of decreasing absorbance coefficient from wavelength 450 nm becomes 400 nm. The annealing temperature is increased band gap of ZnTi is showed by Figure 8b. Increasing band gap indicate crystal growth of compact layer ZnO.

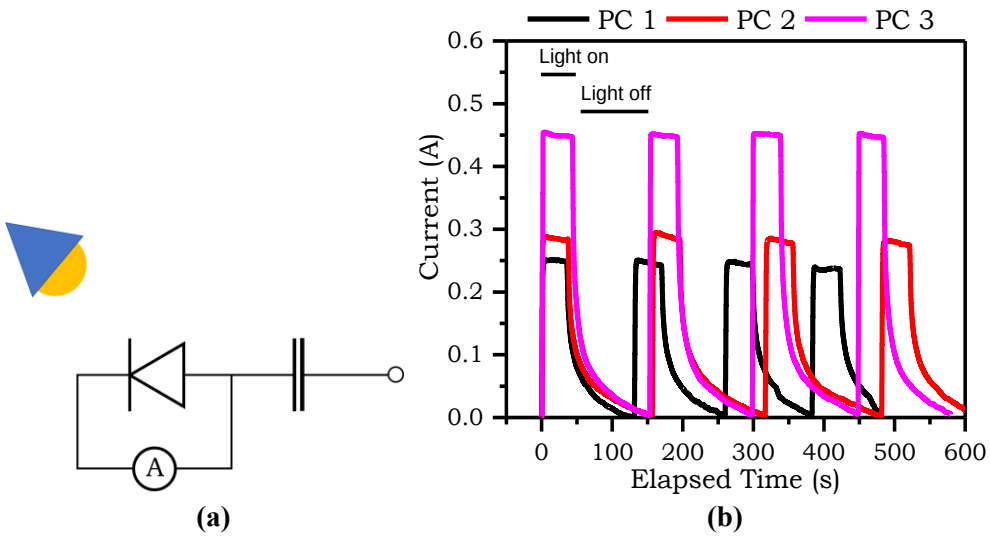

Figure 9. Schematic of photocurrent measurement (a) and I-t graph of photo-supercapacitor (b)

Current vs. elapsed time (I-t) of photo-supercapacitor was measured with the scheme is showed by Figure 9a under 20 mW/cm^2 illumination. Figure 9b shows the photocurrent characteristic of photo-supercapacitor (PC) with various annealing temperature 300, 350, and 400 °C is coded by PC 1, PC 2, and PC 3 respectively. The annealing temperature influence Isc (short-circuit current) of photo-supercapacitor. This corresponds to the crystal growth, energy gap, and the interface between the substrate and metal oxides ZnO and TiO_2. The compact layer ZnO increase interface between mesoporous TiO_2 and FTO substrate that makes electron mobility and photocurrent increase [31,39,40].

Photo-charge of photo-supercapacitor was measured with schematic is showed in Figure 10a. Current vs. elapsed time (I-t) at PC 3 with capacitance supercapacitor 5nF with active area 2 × 1.5 cm^2 is represented by Figure 10b. The constant current charge supercapacitor is 0.423 A. Figure 10c shows photo charge and discharge of supercapacitor is showed by voltage vs. elapsed time (V-t) graph. The charge and discharge of supercapacitor correspond to characteristic decrease exponentially.

Charge-discharge performance of PC 3 corresponds to the transient voltage at series RC circuit [48,49]. Equation 3 express charging while Equation 4 express discharge of the capacitor. Figure 11 shows the voltage vs. elapsed time (V-t) graph and the fitting curve. Voltage maximum Vmax of charging supercapacitor is 40.26 mV with the time constant τ = 15.04 s and potential breakdown is 10 mV that is larger than those in previous work [2]. This is related to the time of charge and discharge in photo-supercapacitor.

$$V_c(t) = V_{\max}\left(1 - \exp\left(-\frac{(t - t_0)}{\tau}\right)\right) \quad (3)$$

$$V_c(t) = V_{\max}\exp\left(-\frac{(t - t_0)}{\tau}\right) \quad (4)$$

where *Vc* is time-dependent capacitor voltage, *Vmax* is saturated voltage, *t* is time, and τ time constant.

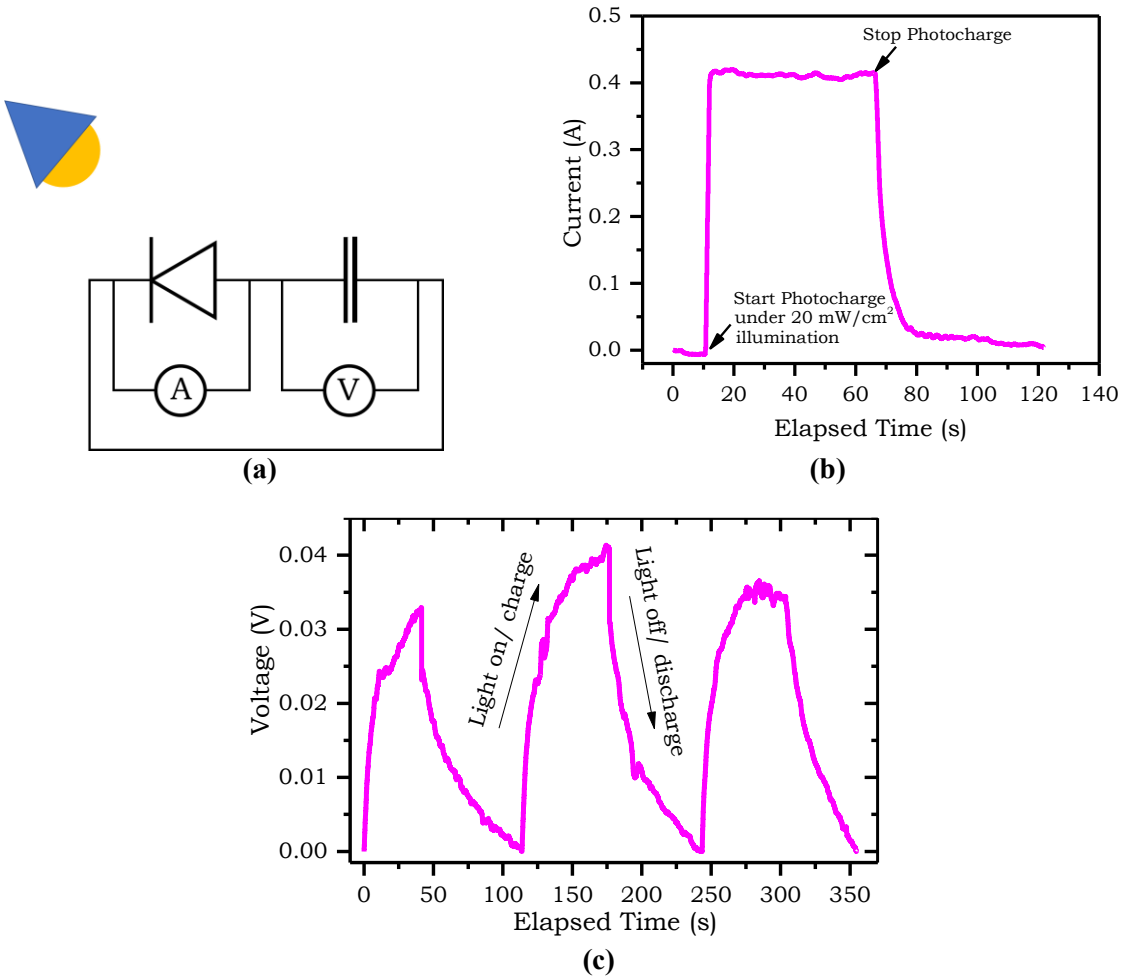

Figure 10. Schematic photocurrent and charge-discharge measurement (a), photocurrent performance (b), and charge-discharge (c) of photo-supercapacitor (PC 3)

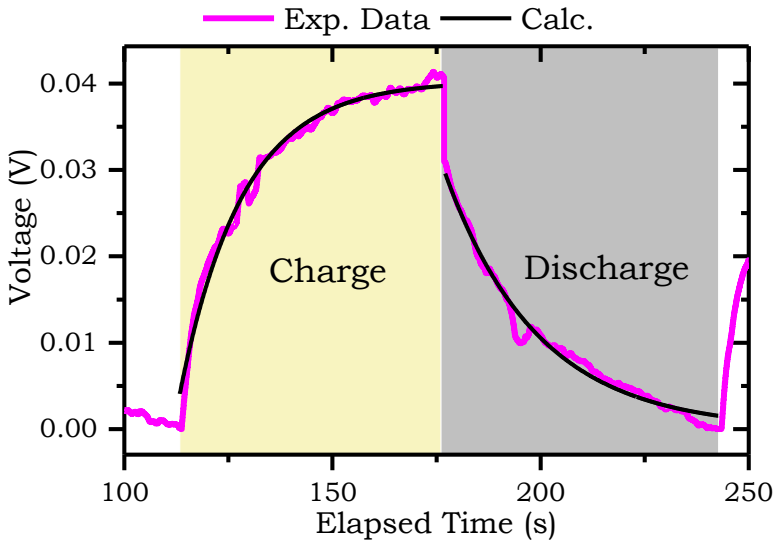

Figure 11. Charge-discharge and fitting curve of capacitor performance for charge and discharge

4. Conclusion

The temperature annealing affects various aspects of photo-supercapacitor performance. This annealing temperature increases the activation energy for crystal growth which improves the interface between the FTO and TiO_2 mesopore. This condition increases the E_g and I_{sc} as well as the stability of the current generated in the photocurrent characteristic.

References

[1] Lau S C, Lim H N, Ravoof T B S A, Yaacob M H, Grant D M, MacKenzie R C I, Harrison I and Huang N M 2017 A three-electrode integrated photo-supercapacitor utilizing graphene-based intermediate bifunctional electrode *Electrochim. Acta* **238** 178–84

[2] Eika E H 2015 *Photocapacitor systems for generation and storage of electrical energy* (University of Bergen, Norway)

[3] Liu R, Liu C and Fan S 2017 A photocapacitor based on organometal halide perovskite and PANI/CNT composites integrated using CNT bridge *J. Mater. Chem. A*

[4] Skunik-Nuckowska M, Grzejszczyk K, Kulesza P J, Yang L, Vlachopoulos N, Häggman L, Johansson E and Hagfeldt A 2013 Integration of solid-state dye-sensitized solar cell with metal oxide charge storage material into photoelectrochemical capacitor *J. Power Sources* **234** 91–9

[5] Miyasaka T and Murakami T N 2004 The photocapacitor: An efficient self-charging capacitor for direct storage of solar energy *Appl. Phys. Lett.* **85** 3932–4

[6] Chen H W, Hsu C Y, Chen J G, Lee K M, Wang C C, Huang K C and Ho K C 2010 Plastic dye-sensitized photo-supercapacitor using electrophoretic deposition and compression methods *J. Power Sources* **195** 6225–31

[7] H.-W. Chen C-Y H, J.-G. Chen, K.-M. Lee, C.-C. Wang K-C H and Ho K-C 2010 Plastic dye-sensitized photo-supercapacitor using electrophoretic deposition and compression methods *J. Power Sources* 6225–31

[8] Murakami T N, Kawashima N and Miyasaka T 2005 A high-voltage dye-sensitized photocapacitor of a three-electrode system *Chem. Commun.* 3346

[9] Bagheri N, Aghaei A, Ghotbi M Y, Marzbanrad E, Vlachopoulos N, Häggman L, Wang M, Boschloo G, Hagfeldt A, Skunik-Nuckowska M and Kulesza P J 2014 Combination of asymmetric supercapacitor utilizing activated carbon and nickel oxide with cobalt polypyridyl-based dye-sensitized solar cell *Electrochim. Acta* **143** 390–7

[10] Scalia A, Varzi A, Lamberti A, Tresso E, Jeong S, Jacob T and Passerini S 2018 High energy and high voltage integrated photo-electrochemical double layer capacitor *Sustain. Energy Fuels* **2** 968–77

[11] Pankove J I and Kiewit D A 1972 Optical Processes in Semiconductors *J. Electrochem. Soc.* **119** 156C

[12] Umale S V., Tambat S N, Sudhakar V, Sontakke S M and Krishnamoorthy K 2017 Fabrication, characterization and comparison of DSSC using anatase TiO_2 synthesized by various methods *Adv. Powder Technol.*

[13] Syafinar R, Gomesh N, Irwanto M, Fareq M and Irwan Y M 2015 Chlorophyll Pigments as Nature Based Dye for Dye-Sensitized Solar Cell (DSSC) *Energy Procedia* **79** 896–902

[14] Pugazhendhi K, D'Almeida S, Kumar P N, Mary J S S, Tenkyong T, Sharmila D J, J M and Shyla J M 2018 Hybrid TiO_2/ZnO and TiO_2/Al plasmon impregnated ZnO nanocomposite photoanodes for DSSCs: synthesis and characterisation *Mater. Res. Express* **5** 045053

[15] Shi Y, Wang K, Du Y, Zhang H, Gu J, Zhu C, Wang L, Guo W, Hagfeldt A and Wang N 2013 Solid-State Synthesis of ZnO Nanostructures for Quasi-Solid Dye-Sensitized Solar Cells with High Efficiencies up to 6.46% *Adv. Mater.* **25** 4413–4419

[16] An H-R, An H, Riu D-H and Ahn H-J 2015 Improved Photovoltaic Properties Of Dye-Sensitized Solar Cells Using Laser Patterned F-Doped SnO2 Thin Films *Arch. Metall. Mater.* **60** 1241–1245

[17] Zhao X G, Park J-Y, Jin E M and Gu H-B 2015 Tuning the Interfacial Area and Porosity of TiO_2 Film for Enhanced Light Harvesting in DSSC *J. Electrochem. Soc.* **162** E1–E6

[18] Miles D O, Lee C S, Cameron P J, Mattia D and Kim J H 2016 Hierarchical growth of TiO_2 nanosheets on anodic ZnO nanowires for high efficiency dye-sensitized solar cells *J. Power Sources* **325** 365–74
[19] Ranasinghe C S K, Jayaweera E N, Kumara G R A, Rajapakse R M G, Onwona-Agyeman B, Perera A G U and Tennakone K 2015 Tin oxide based dye-sensitized solid-state solar cells: surface passivation for suppression of recombination *Mater. Sci. Semicond. Process.* **40** 890–5
[20] Diantoro M, Suprayogi T, Hidayat A, Taufiq A, Fuad A and Suryana R 2018 Shockley ' s Equation Fit Analyses for Solar Cell Parameters from I-V Curves **2018**
[21] Diantoro M, Masrul M Z and Taufiq A 2018 Effect of TiO_2 Nanoparticles on Conductivity and Thermal Stability of PANI-TiO_2/Glass Composite Film *J. Phys. Conf. Ser.* **1011** 012065
[22] Sengupta D, Das P, Mondal B and Mukherjee K 2016 Effects of doping, morphology and film-thickness of photo-anode materials for dye sensitized solar cell application – A review *Renew. Sustain. Energy Rev.* **60** 356–76
[23] Li K-N, Wang Y-F, Xu Y-F, Chen H-Y, Su C-Y and Kuang D-B 2013 Macroporous SnO_2 Synthesized via a Template-Assisted Reflux Process for Efficient Dye-Sensitized Solar Cells *ACS Appl. Mater. Interfaces* **5** 5105–5111
[24] Liao J-Y, He J-W, Xu H, Kuang D-B and Su C-Y 2012 Effect of TiO_2 morphology on photovoltaic performance of dye-sensitized solar cells: nanoparticles, nanofibers, hierarchical spheres and ellipsoid spheres *J. Mater. Chem.* **22** 7910–7918
[25] Chao C-H, Chang C-L, Chan C-H, Lien S-Y, Weng K-W and Yao K-S 2010 Rapid thermal melted TiO_2 nano-particles into ZnO nano-rod and its application for dye sensitized solar cells *Thin Solid Films* **518** 7209–7212
[26] Sun X, Zhang Q, Liu Y, Huang N, Sun P, Peng T, Peng T and Zhao X-Z 2014 Photovoltaic performance improvement of dye-sensitized solar cells through introducing In-doped TiO_2 film at conducting glass and mesoporous TiO_2 interface as an efficient compact layer *Electrochim. Acta* **129** 276–82
[27] Zhao D, Peng T, Lu L, Cai P, Jiang P and Bian Z 2008 Effect of Annealing Temperature on the Photoelectrochemical Properties of Dye-Sensitized Solar Cells Made with Mesoporous TiO_2 Nanoparticles *J. Phys. Chem. C* **112** 8486–94
[28] Chen X, Du Q, Yang W, Liu W, Miao Z and Yang P 2018 A double-layered photoanode made of ZnO/TiO_2 composite nanoflowers and TiO_2 nanorods for high efficiency dye-sensitized solar cells *J. Solid State Electrochem.* **22** 685–91
[29] Senthil T S, Muthukumarasamy N and Kang M 2013 Applications of highly ordered paddle wheel like structured ZnO nanorods in dye sensitized solar cells *Mater. Lett.* **102**–**103** 26–9
[30] Bai Y, Yu H, Li Z, Amal R, Lu G Q M and Wang L 2012 In Situ Growth of a ZnO Nanowire Network within a TiO_2 Nanoparticle Film for Enhanced Dye-Sensitized Solar Cell Performance *Adv. Mater.* **24** 5850–6
[31] Huang J-J, Chiu S-P, Wu M-J and Hsu C-F 2016 Effect of titanium oxide compact layer in dye-sensitized solar cell prepared by liquid-phase deposition *Appl. Phys. A* **122** 971
[32] Kulkarni S S, Belavi P B and Khadke U V. 2018 Synthesis, structural, characterization and dielectric spectroscopy of PVDF – BaTiO3 polymer composite *AIP Conference Proceedings* p 090046
[33] Ben Cheikh Z, El Kamel F, Gallot-Lavallée O, Soussou M A, Vizireanu S, Achour A and Khirouni K 2017 Hydrogen doped $BaTiO_3$ films as solid-state electrolyte for micro-supercapacitor applications *J. Alloys Compd.* **721** 276–84
[34] N. Bagheri A A, M.Y. Ghotbi E M, N. Vlachopoulos L H, M. Wang G B and A. Hagfeldt M S N 2014 Combination of asymmetric supercapacitor utilizing activated carbon and nickel oxide with cobalt polypyridyl-based dye-sensitized solar cell *Electrochim. Acta* 390–7
[35] Weirich T E, Winterer M, Seifried S and Mayer J 2002 Structure of nanocrystalline anatase solved and refined from electron powder data *Acta Crystallogr. Sect. A Found. Crystallogr.* **58** 308–15

[36] Kihara K and Donnay G 1985 Anharmonic thermal vibrations in ZnO *Can. Mineral.* **23** 647–54
[37] Kumara G R A, Deshapriya U, Ranasinghe C S K, Jayaweera E N and Rajapakse R M G 2018 Efficient dye-sensitized solar cells from mesoporous zinc oxide nanostructures sensitized by N719 dye *J. Semicond.* **39** 1–6
[38] Ismail A A and Mazyck D W 2008 Impact of Heat Treatment and Composition of ZnO−TiO_2 Nanoparticles for Photocatalytic Oxidation of an Azo Dye *Ind. Eng. Chem. Res.* **47** 1483–7
[39] Chou J, Lin Y, Liao Y, Lai C-H, Chu C-M, You P-H and Nien Y-H 2016 Photovoltaic Performance Analysis of Dye-Sensitized Solar Cell With ZnO Compact Layer and TiO_2 /Graphene Oxide Composite Photoanode *IEEE J. Electron Devices Soc.* **4** 402–9
[40] Yang Y, Peng X, Chen S, Lin L, Zhang B and Feng Y 2014 Performance improvement of dye-sensitized solar cells by introducing a hierarchical compact layer involving ZnO and TiO2blocking films *Ceram. Int.* **40** 15199–206
[41] Abdullah M and Khairurrijal K 2009 A simple method for determining surface porosity based on SEM images using OriginPro software *Indones. J. Phys.* **20** 37–40
[42] Mustikasari A A, Diantoro M, Mufti N and Suryana R 2018 The Effect Of Nano ZnO Morphology on Structure, Dielectric Constant, and Dissipation Factor Of CA-Nano ZnO/ITO Films *J. Neutrino* **10** 65
[43] Caglar M, Ilican S and Caglar Y 2009 Influence of dopant concentration on the optical properties of ZnO: In films by sol–gel method *Thin Solid Films* **517** 5023–8
[44] Kurda A H, Hassan Y M and Ahmed N M 2015 Controlling Diameter, Length and Characterization of ZnO Nanorods by Simple Hydrothermal Method for Solar Cells *World J. Nano Sci. Eng.* **05** 34
[45] Abd Elkader O 2012 Preparation and characterization of nanostructured zinc oxide thin films *AIP Conference Proceedings* vol 539 pp 539–42
[46] Islam M A 2012 Optical and Structural Characterization of TiO_2 Nanoparticles *IOSR J. Electr. Electron. Eng.* **3** 18–24
[47] Ardhani N ., Supriyanto A ., Yuwono A H . and Suryana R . 2014 Influence of mass ratio of aquadest and TTIP on the synthesis of TiO_2 nanoparticles to improve the performance of DSSC with beta-carotene as sensitizer *Adv. Mater. Res.* **896** 481–4
[48] Devillers N, Jemei S, Péra M-C, Bienaimé D and Gustin F 2014 Review of characterization methods for supercapacitor modelling *J. Power Sources* **246** 596–608
[49] Quintans C, Iglesias R, Lago A, Acevedo J M and Martinez-Penalver C 2017 Methodology to Obtain the Voltage-Dependent Parameters of a Fourth-Order Supercapacitor Model With the Transient Response to Current Pulses *IEEE Trans. Power Electron.* **32** 3868–78

Acknowledgments
This research was partially funded by INSINAS 2018 scheme of KEMENRISTEKDIKTI.